

# **A COMPARISON OF COARSE MESH REBALANCE AND COARSE MESH FINITE DIFFERENCE ACCELERATIONS FOR THE NEUTRON TRANSPORT CALCULATIONS**

**Nam Zin Cho and Chang Je Park**

Korea Advanced Institute of Science and Technology  
373-1 Kusong-dong, Yusong-gu, Taejon, Korea 305-701  
nzcho@mail.kaist.ac.kr

## **ABSTRACT**

This paper provides Fourier stability/convergence analysis of the coarse mesh finite difference (CMFD) acceleration method, compared to that of the coarse mesh rebalance (CMR) method. The results show that CMFD is also conditionally stable as is CMR. The behavior of its spectral radius is similar to that of the inconsistent diffusion synthetic acceleration (DSA). The CMFD method is fast converging when the mesh size is small as is DSA, but it becomes divergent or ineffective as the mesh size increases as does CMR. The numerical results on several test problems are in good agreement with the Fourier analysis.

*Key Words:* acceleration, Fourier analysis, CMR, CMFD, inconsistent DSA

## **1. INTRODUCTION**

As the reactor core becomes more complicated, there is growing need to perform three-dimensional whole-core heterogeneous transport calculations [1,2], which require many iterations and long computing times. Among many acceleration methods for neutron transport calculations, the coarse mesh rebalance (CMR) acceleration method is extremely simple to apply regardless of the discretization schemes for the transport solution.[3,4] Although it is not unconditionally convergent and it is a nonlinear method, it is easily linearized and its convergence properties are Fourier-analyzable. It does not involve interim solutions in the denominators and thus it should be numerically robust, unlike many other nonlinear methods, and if it converges, it does so to the unaccelerated solution, i.e., it is a true acceleration method. The CMR adjusts the average amplitude of the flux over each coarse volume while leaving the detailed space-angle distribution of the flux within the coarse mesh unchanged. This complements nicely the iteration on the scattering source, which corrects details in the space-angle distribution rapidly but is poor in eliminating components of the error that extend over large spatial domains.[3]

The so-called coarse mesh finite difference (CMFD) acceleration method is popular especially for the fast solutions of nodal diffusion equations.[5]-[7] Recently, this CMFD method has been employed for the acceleration of the 2-D transport calculation in the CASMO-4 code[8,9] with remarkable results. Similar works are reported in Refs. 10 and 11. In the CMFD method, a current correction coefficient is introduced to preserve the interface currents between coarse meshes, which are results from the solutions of transport sweep.

In this paper, we present a comparison of the convergence and stability properties of the two acceleration methods. Since both methods are nonlinear, they are linearized and then Fourier-analyzed. The convergence analysis of the CMR method is already available in the literature but is included here for completeness. The convergence analysis of the CMFD method is, however, presented here for the first time to the best of our knowledge.

## 2. CMR AND CMFD METHODS IN SLAB GEOMETRY

### 2.1. Equations of Coarse Mesh Rebalance (CMR) Method

In the slab geometry, the neutron transport equation is written as follows:

$$\mu \frac{d}{dx} \psi^{l+1/2}(x, \mu) + \sigma(x) \psi^{l+1/2}(x, \mu) = \sigma_s(x) \phi^l(x) + q(x), \quad (1)$$

where the standard notations are used and  $l$  denotes the iteration index.[3]

To derive the CMR equations, let us consider a coarse mesh which contains several fine meshes as shown in Fig. 1.

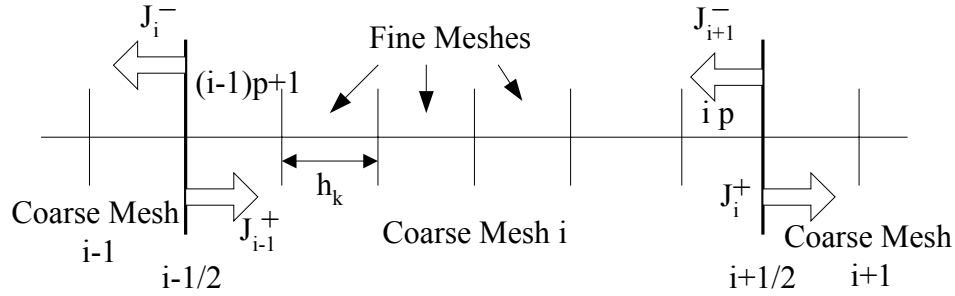


**Fig.1. Configuration of coarse meshes and fine meshes in slab geometry.**

When angular integration and spatial integration over the coarse mesh are performed, we obtain the following equation:

$$\left( J_i^{+,l+1/2} + J_i^{-,l+1/2} + \sum_k h_k (\sigma_{ki} - \sigma_{s,ki}) \phi_{ki}^{l+1/2} \right) - J_{i-1}^{+,l+1/2} - J_{i+1}^{-,l+1/2} = \sum_k h_k q_{ki}, \quad (2)$$

where

$$J_i^{+,l+1/2} = \frac{1}{2} \sum_{n=1}^{N/2} w_n |\mu_n| \psi_{n,i+1/2}^{l+1/2}, \quad \mu_n > 0, \quad (3)$$

$$J_i^{-,l+1/2} = \frac{1}{2} \sum_{n=N/2+1}^N w_n |\mu_n| \psi_{n,i-1/2}^{l+1/2}, \quad \mu_n < 0, \quad (4)$$

$i$  denotes coarse mesh and  $k$  fine mesh, and  $(\mu_n, w_n)$  are the discrete ordinates quadrature set.

Following the standard procedure, we first change all the indices in Eq. (2) into  $l+1$ . Then the rebalance factor,  $f_i$ , is defined on coarse mesh  $i$  and it is allowed to be discontinuous at the interfaces between coarse meshes. Since neutrons contributing to  $J_i^+$  are leaving the coarse mesh

$i$  we use  $f_i$ , and for  $J_{i+1}^-$ , whose neutrons are from the coarse mesh  $i+1$  to the coarse mesh  $i$  we use  $f_{i+1}$ :

$$\psi_{n,i+1/2}^{l+1} = f_i^{l+1} \psi_{n,i+1/2}^{l+1/2}, \quad \mu_n > 0, \quad (5)$$

$$\psi_{n,i+1/2}^{l+1} = f_{i+1}^{l+1} \psi_{n,i+1/2}^{l+1/2}, \quad \mu_n < 0. \quad (6)$$

The CMR equation for slab geometry is then derived easily as

$$\left( J_i^{+,l+1/2} + J_i^{-,l+1/2} + \sum_k h_k (\sigma_{ki} - \sigma_{s,ki}) \phi_{ki}^{l+1/2} \right) f_i^{l+1} - J_{i-1}^{+,l+1/2} f_{i-1}^{l+1} - J_{i+1}^{-,l+1/2} f_{i+1}^{l+1} = \sum_k h_k q_{ki}. \quad (7)$$

If the vacuum boundary condition is imposed on the left side (coarse mesh 1), then  $J_0^+ = 0$  and the CMR equation is given as

$$\left( J_1^{+,l+1/2} + J_1^{-,l+1/2} + \sum_k h_k (\sigma_{k1} - \sigma_{s,k1}) \phi_{k1}^{l+1/2} \right) f_1^{l+1} - J_2^{-,l+1/2} f_2^{l+1} = \sum_k h_k q_{k1}. \quad (8)$$

If the reflective boundary condition is given on the right side (coarse mesh I), then  $J_I^+ = J_{I+1}^-$  and  $f_I = f_{I+1}$ . Thus, the CMR equation is derived as

$$\left( J_I^{-,l+1/2} + \sum_k h_k (\sigma_{kl} - \sigma_{s,kl}) \phi_{kl}^{l+1/2} \right) f_I^{l+1} - J_{I-1}^+ f_{I-1}^{l+1} = \sum_k h_k q_{kl}. \quad (9)$$

If the reflective boundary conditions are given on both sides of the problem, the incoming boundary angular flux should be updated on each iteration as follows:

$$\psi_{n,1/2}^{l+1} = f_1^{l+1} \psi_{N+1-n,1/2}^{l+1/2}, \quad \mu_n > 0 \quad (n = 1, \dots, N/2), \quad (10)$$

$$\psi_{n,I+1/2}^{l+1} = f_I^{l+1} \psi_{N+1-n,I+1/2}^{l+1/2}, \quad \mu_n < 0 \quad (n = N/2 + 1, \dots, N). \quad (11)$$

As the solution converges, the rebalance factor  $f_i$  approaches unity, so the detailed balance is satisfied in CMR.

## 2.2. Equations of Coarse Mesh Finite Difference (CMFD) Method

The form of CMFD equations is similar to that of the usual finite difference equation with a mesh-centered scheme, but there is an additional current correction factor,  $\hat{D}$ , which is defined as[8]-[11]

$$\hat{D}_{i+1/2} = -\frac{J_{i+1/2}^{l+1/2} + \tilde{D}_{i+1/2} (\phi_{i+1}^{l+1/2} - \phi_i^{l+1/2})}{\phi_{i+1}^{l+1/2} + \phi_i^{l+1/2}}, \quad (12)$$

where

$$\tilde{D}_{i+1/2} = 2 \frac{(D_i/h_i)(D_{i+1}/h_{i+1})}{D_i/h_i + D_{i+1}/h_{i+1}}, \quad (13)$$

$$J_{i+1/2}^{l+1/2} = \frac{1}{2} \sum_{n=1}^N w_n \mu_n \psi_{n,i+1/2}^{l+1/2}. \quad (14)$$

The CMFD equation for coarse mesh  $i$  with current correction factors is

$$\begin{aligned} & -\tilde{D}_{i+1/2} (\phi_{i+1}^{l+1} - \phi_i^{l+1}) - \hat{D}_{i+1/2} (\phi_{i+1}^{l+1} + \phi_i^{l+1}) + \tilde{D}_{i-1/2} (\phi_i^{l+1} - \phi_{i-1}^{l+1}) + \hat{D}_{i-1/2} (\phi_i^{l+1} + \phi_{i-1}^{l+1}) \\ & + \sum_k h_k (\sigma_k - \sigma_{sk}) \phi_{ki}^{l+1} = \sum_k h_k q_{ki}. \end{aligned} \quad (15)$$

Rewriting Eq. (15), we obtain

$$\begin{aligned}
 & -(\tilde{D}_{i+1/2} + \hat{D}_{i+1/2})\phi_{i+1}^{l+1} - (\tilde{D}_{i-1/2} - \hat{D}_{i-1/2})\phi_{i-1}^{l+1} \\
 & + (\tilde{D}_{i+1/2} - \hat{D}_{i+1/2} + \tilde{D}_{i-1/2} + \hat{D}_{i-1/2} + h_i \sigma_{ai})\phi_i^{l+1} = \sum_k h_k q_k,
 \end{aligned} \tag{16}$$

where  $\phi_i^{l+1} = \frac{1}{h_i} \sum_k h_k \phi_{ki}^{l+1}$ .

If the vacuum boundary condition is given on the left side (coarse mesh 1), then  $J_{1/2}^+ = 0$  so that

$$\begin{aligned}
 J_{1/2}^{l+1/2} &= -\hat{D}_{1/2}(\phi_1^{l+1/2} + \phi_0^{l+1/2}) - \tilde{D}_{1/2}(\phi_1^{l+1/2} - \phi_0^{l+1/2}) \\
 &= \frac{1}{2} \sum_{n=1}^N w_n \mu_n \psi_{n,1/2}^{l+1/2} = 0 + \frac{1}{2} \sum_{n=N/2+1}^N w_n \mu_n \psi_{n,1/2}^{l+1/2}.
 \end{aligned} \tag{17}$$

The CMFD equation with vacuum boundary condition is then derived as, using the mesh average scalar fluxes of coarse mesh 1,

$$\begin{aligned}
 & -(\tilde{D}_{3/2} + \hat{D}_{3/2})\phi_2^{l+1} + (\tilde{D}_{3/2} - \hat{D}_{3/2} + h_1(\sigma_1 - \sigma_{s1}))\phi_1^{l+1} \\
 & - \left( \frac{1}{2} \sum_{n=N/2+1}^N w_n \mu_n \psi_{n,1/2}^{l+1/2} \right) \frac{\phi_1^{l+1}}{\phi_1^{l+1/2}} = \sum_k h_k q_{k1}.
 \end{aligned} \tag{18}$$

The use of a ratio of the mesh average scalar fluxes in Eq. (18) comes from the concept of the CMR factor.

If the reflective boundary condition is given on the right side (coarse mesh I), then  $J_I = 0$  so that

$$J_{I+1/2}^{l+1/2} = -\hat{D}_{I+1/2}(\phi_{I+1}^{l+1/2} + \phi_I^{l+1/2}) - \tilde{D}_{I+1/2}(\phi_{I+1}^{l+1/2} - \phi_I^{l+1/2}) = 0. \tag{19}$$

Thus, the CMFD equation with reflective boundary condition is given as

$$(\tilde{D}_{I-1/2} - \hat{D}_{I-1/2})\phi_{I-1}^{l+1} + (\tilde{D}_{I-1/2} + \hat{D}_{I-1/2} + h_I(\sigma_I - \sigma_{sI}))\phi_I^{l+1} = \sum_k h_k q_{kI}. \tag{20}$$

In the case of the reflective boundary conditions on both sides, the incoming angular flux is updated using the coarse-mesh average scalar fluxes:

$$\psi_{n,1/2}^{l+1} = \frac{\phi_1^{l+1}}{\phi_1^{l+1/2}} \psi_{N+1-n,1/2}^{l+1/2}, \quad \mu_n > 0 \quad (n=1, \dots, N/2), \tag{21}$$

$$\psi_{n,I+1/2}^{l+1} = \frac{\phi_I^{l+1}}{\phi_I^{l+1/2}} \psi_{N+1-n,I+1/2}^{l+1/2}, \quad \mu_n < 0 \quad (n=N/2+1, \dots, N). \tag{22}$$

### 3. CONVERGENCE ANALYSES OF CMR AND CMFD

To investigate convergence or stability of some acceleration methods, Fourier analysis is widely used. To begin Fourier analysis, nonlinear methods should be linearized and a model problem of an infinite medium, constant cross section, and flat source with a uniform mesh is considered.

Then the Fourier ansatz is applied, which has the standard Fourier component  $[\exp(j\lambda x), j = \sqrt{-1}]$  and the eigenvalue( $\omega$ ). The spectral radius( $\rho$ ) is the maximum of the eigenvalues. If  $\rho < 1$ , the method is stable.

#### 3.1. Fourier Analysis of CMR

In the case of CMR, a detailed stability analysis was performed by Cefus and Larsen.[12] They

provide a procedure of linearization to accomplish analysis of the CMR method, which is originally nonlinear. In the derivation, diamond differenced high-order equation is used. For the general coarse mesh rebalance ( $p$  fine meshes per coarse mesh), they derived an eigenvalue problem in a form:

$$\omega \mathbf{A} = [\mathbf{H} - \eta \mathbf{U} \mathbf{V} \cdot (\mathbf{I} - \mathbf{H})] \mathbf{A} = \mathbf{L}_{CMR} \mathbf{A}, \quad (23)$$

where

$$\mathbf{A} = [A_{(i-1)p+1} \cdots A_{(i-1)p}]^T, \quad (24a)$$

$$\mathbf{M} = \begin{pmatrix} 0 & 1 & & 0 \\ & 0 & 1 & \\ & & \cdot & \cdot \\ & & & 1 \\ 1 & & & 0 \end{pmatrix}, \quad \mathbf{I} = \begin{pmatrix} 1 & 0 & & 0 \\ & 1 & 0 & \\ & \cdot & \cdot & \cdot \\ & & & 1 \\ 0 & & & 1 \end{pmatrix}, \quad (24b)$$

$$\mathbf{K} = \frac{1}{j} [\exp(j\tau) \mathbf{M} - \exp(-j\tau) \mathbf{I}] \times [\exp(j\tau) \mathbf{M} + \exp(-j\tau) \mathbf{I}]^{-1}, \quad (24c)$$

$$\mathbf{H} = \frac{c}{2} \sum_{n=1}^N w_n [\mathbf{I} + (2\mu_n / h)^2 \mathbf{K} \cdot \mathbf{K}]^{-1}, \quad (24d)$$

$$\mathbf{V} = [\exp(j\tau(1-p)) \cdots \exp(j\tau(p-1))], \quad \mathbf{U} = [\exp(j\tau(p-1)) \cdots \exp(j\tau(1-p))]^T, \quad (24e)$$

$$\eta = \frac{hc}{2\gamma \sin^2(p\tau) + ph(1-c)}, \quad \tau = \frac{\lambda h}{2}, \quad c = \frac{\sigma_s}{\sigma}, \quad \gamma = \sum_{n=1}^{N/2} \mu_n w_n. \quad (24f)$$

The spectral radius( $\rho$ ) is

$$\rho = \sup_{\tau} |\omega(\tau)|. \quad (25)$$

For the case of fine mesh rebalance ( $p=1$ ), the eigenvalue( $\omega$ ) is expressed explicitly as

$$\omega = 1 - (1 - \kappa) \left\{ 1 + \frac{hc}{2\gamma \sin^2(\tau) + h(1-c)} \right\}, \quad (26)$$

where

$$\kappa = \frac{c}{2} \sum_{n=1}^N w_n / \{ ((2\mu_n \tan \tau) / h)^2 + 1 \}. \quad (27)$$

Figs. 2, 3, and 4 show the spectral radii of CMR for various scattering ratios when  $p=1$ ,  $p=2$ , and  $p=4$ , respectively, using the  $S_{16}$  Gauss-Legendre quadrature set. Since the Fourier analysis is performed after linearization around the solution of an infinite medium problem, it does not apply to the case of  $c=1$ . Therefore, we have chosen values for  $c$  upto 0.9999. It is indicated that for given  $c$ , when  $p=1$ , CMR is unstable for  $\sigma h$  too small or too large. The case of a large  $p$  is generally more stable compared to the case of  $p=1$ , especially for thick mesh sizes.

### 3.2. Fourier Analysis of CMFD

This section describes the procedure of Fourier analysis of CMFD. For the high-order equations, the diamond differencing (DD) scheme is used as

$$\mu_n \frac{\psi_{k+1/2}^{l+1/2} - \psi_{k-1/2}^{l+1/2}}{h} + \sigma \frac{\psi_{k+1/2}^{l+1/2} + \psi_{k-1/2}^{l+1/2}}{2} = \sigma_s \phi_k^l + Q, \tag{28}$$

$$\phi_k^{l+1/2} = \frac{1}{2} \sum_{n=1}^N w_n \frac{\psi_{k+1/2}^{l+1/2} + \psi_{k-1/2}^{l+1/2}}{2}. \tag{29}$$

If the medium is infinite with constant cross sections and uniform meshes, the low-order equations of the CMFD method are given by

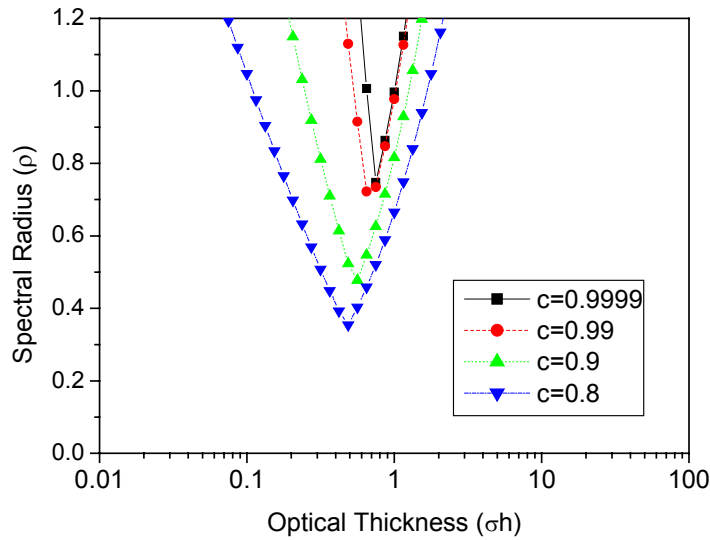


Fig. 2. Spectral radius of CMR for various scattering ratios for p=1.

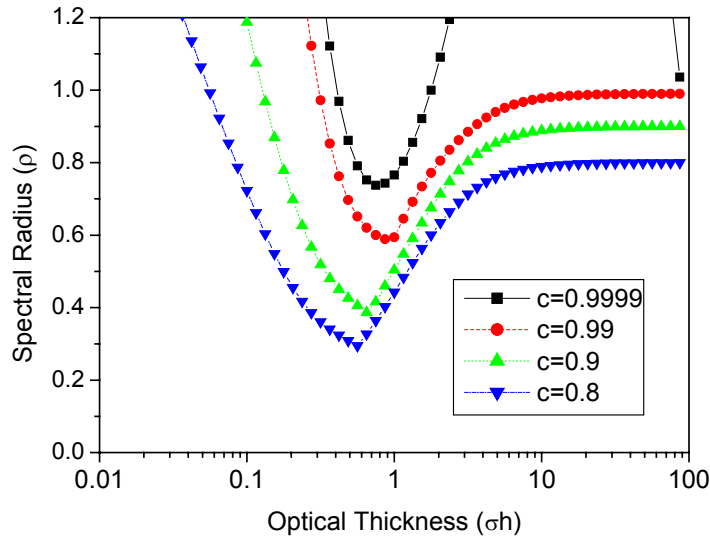
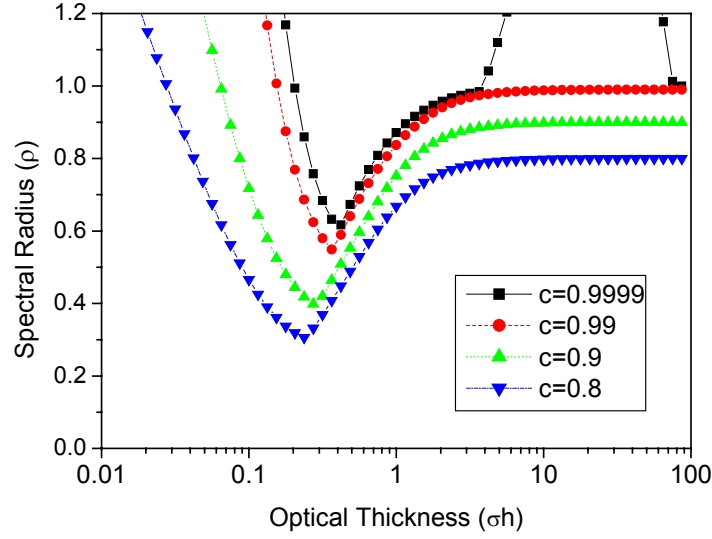


Fig. 3. Spectral radius of CMR for various scattering ratios for p=2.



**Fig. 4. Spectral radius of CMR for various scattering ratios for  $p=4$ .**

$$\begin{aligned}
 & -(\tilde{D}_{i+1/2} + \hat{D}_{i+1/2})\phi_{i+1}^{l+1} - (\tilde{D}_{i-1/2} - \hat{D}_{i-1/2})\phi_{i-1}^{l+1} \\
 & + (\tilde{D}_{i+1/2} - \hat{D}_{i+1/2} + \tilde{D}_{i-1/2} + \hat{D}_{i-1/2} + hp\sigma_a)\phi_i^{l+1} = phQ,
 \end{aligned} \tag{30}$$

$$\phi_k^{l+1} = \phi_k^{l+1/2} \frac{\phi_i^{l+1}}{\frac{1}{p} \sum_k \phi_k^{l+1/2}}, \tag{31}$$

where

$$\sigma = 1, \quad \sigma_s = c, \tag{32a}$$

$$\tilde{D}_{i+1/2} = 2 \frac{(D_i/h_i)(D_{i+1}/h_{i+1})}{D_i/h_i + D_{i+1}/h_{i+1}} = D/(ph) = 1/(3\sigma ph) = 1/(3ph), \tag{32b}$$

$$\hat{D}_{i+1/2} = -\frac{J_{i+1/2}^{l+1/2} + (\phi_{i+1}^{l+1/2} - \phi_i^{l+1/2})/(3ph)}{\phi_{i+1}^{l+1/2} + \phi_i^{l+1/2}}, \tag{32c}$$

$$\phi_i^{l+1} = \frac{1}{p} \sum_{k \in i} \phi_k^{l+1}, \tag{32d}$$

$$J_{i+1/2}^{l+1/2} = \frac{1}{2} \sum_{n=1}^N w_n \mu_n \psi_{n,i+1/2}^{l+1/2}. \tag{32e}$$

The CMFD method is nonlinear, so the CMFD equations are linearized around the solution of the model problem. If we define the following ansatz for linearization:

$$\phi_i^{l+1} = Q/\sigma_a(1 + \varepsilon \zeta_i^{l+1}), \tag{33}$$

$$\phi_i^{l+1/2} = Q/\sigma_a(1 + \varepsilon \zeta_i^{l+1/2}), \tag{34}$$

$$\psi_{i+1/2}^{l+1/2} = Q/\sigma_a(1 + \varepsilon \zeta_{n,i+1/2}^{l+1/2}), \tag{35}$$

and choose the  $O(\varepsilon)$  term, the following linear equations are obtained after some algebra:

$$\mu_n \frac{\xi_{n,k+1/2}^{l+1/2} - \xi_{n,k-1/2}^{l+1/2}}{h} + \frac{\xi_{n,k+1/2}^{l+1/2} + \xi_{n,k-1/2}^{l+1/2}}{2} = c \zeta_k^l, \quad (36)$$

$$\zeta_k^{l+1/2} = \frac{1}{2} \sum_{n=1}^N w_n \frac{\xi_{n,k+1/2}^{l+1/2} + \xi_{n,k-1/2}^{l+1/2}}{2}, \quad (37)$$

$$\begin{aligned} & -\frac{1}{3ph} \zeta_{i+1}^{l+1} + \frac{2}{3ph} \zeta_i^{l+1} - \frac{1}{3ph} \zeta_{i-1}^{l+1} + hp \sigma_a \zeta_i^{l+1} \\ & = -\frac{1}{3ph} \zeta_{i+1}^{l+1/2} + \frac{2}{3ph} \zeta_i^{l+1/2} - \frac{1}{3ph} \zeta_{i-1}^{l+1/2} + h \sigma_a \sum_k \zeta_k^{l+1/2} + h \sigma_s \sum_k (\zeta_k^{l+1/2} - \zeta_k^l), \end{aligned} \quad (38)$$

$$\zeta_k^{l+1} = \zeta_k^{l+1/2} + \zeta_i^{l+1} - \frac{1}{p} \sum_k \zeta_k^{l+1/2}. \quad (39)$$

The  $O(1)$  terms are automatically satisfied and the  $O(\varepsilon^2)$  terms are neglected. When Eq. (38) is derived the following balance equation was used, which was also used to linearize the CMR equation:

$$\frac{1}{2} \sum_{n=1}^N w_n \mu_n (\xi_{n,i+1/2}^{l+1/2} - \xi_{n,i-1/2}^{l+1/2}) - h \sigma \sum_k \zeta_k^{l+1/2} = h \sigma_s \sum_k \zeta_k^l. \quad (40)$$

We note that Eq. (38) is in the same form as the inconsistent diffusion synthetic acceleration (DSA) equation. Thus, it is expected that the convergence of the CMFD method may be similar to that of the inconsistent DSA method.

In the case of a uniform mesh and an infinite medium, the following Fourier ansatz are appropriate:

$$\zeta_i^l = \omega^l A \exp(j\lambda x_i), \quad (41)$$

$$\zeta_k^l = \omega^l A_k \exp(j\lambda x_k), \quad A_k = A_{k+p}, \quad (42)$$

$$\zeta_i^{l+1/2} = \omega^l B \exp(j\lambda x_i), \quad (43)$$

$$\zeta_k^{l+1/2} = \omega^l B_k \exp(j\lambda x_k), \quad B_k = B_{k+p}, \quad (44)$$

$$\xi_{n,k+1/2}^{l+1/2} = \omega^l a_{n,k} \exp(j\lambda x_{k+1/2}), \quad a_{n,k} = a_{n,k+p}. \quad (45)$$

Introducing these Fourier ansatz into Eqs. (36) and (37), the Fourier components cancel out. The high-order equations (Eqs. (36) and (37)) are rewritten in the following matrix form, interestingly in a similar form of the CMR method:

$$\mathbf{B} = \mathbf{H} \mathbf{A}, \quad (46)$$

where  $\mathbf{B} = [B_{(i-1)p+1} \cdots B_{(i-1)p}]^T$ ,  $\mathbf{A} = [A_{(i-1)p+1} \cdots A_{(i-1)p}]^T$ . The matrix  $\mathbf{H}$  was already defined in Eq. (24d).

Rewriting Eq. (38) using the Fourier ansatz,

$$\begin{aligned} \left\{ \frac{2}{3ph} + hp \sigma_a - \frac{2}{3ph} \cos(2p\tau) \right\} \omega A &= \left\{ \frac{2}{3ph} + hp \sigma_a - \frac{2}{3ph} \cos(2p\tau) \right\} B \\ &+ hc \sum_k U(k) (B_k - A_k), \end{aligned} \quad (47)$$

where

$$U(k) = \exp(j(2p-1-2k)). \quad (48)$$

Eq. (39) is rewritten as



$$U(k)\omega A_k = U(k)B_k + \omega A - \frac{1}{p} \sum_k U(k)B_k = U(k)B_k + \omega A - B, \tag{49}$$

where

$$B = \frac{1}{p} \sum_k U(k)B_k. \tag{50}$$

Combining Eqs. (47) and (49), the following eigenvalue problem is obtained:

$$\omega \mathbf{A} = [\mathbf{H} - \theta \mathbf{UV} \cdot (\mathbf{I} - \mathbf{H})] \mathbf{A} = \mathbf{L}_{CMFD} \mathbf{A}, \tag{51}$$

where

$$\theta = hc / [\{4 \sin^2(p\tau)\} / (3ph) + hp(1-c)]. \tag{52}$$

For the case of fine mesh rebalance (p=1), the eigenvalue(  $\omega$  ) is expressed explicitly as

$$\omega = 1 - (1 - \kappa) \left\{ 1 + \frac{hc}{(4 \sin^2 \tau) / (3h) + h(1-c)} \right\}. \tag{53}$$

It is interesting to note that the eigenvalue equations of CMR and CMFD methods have the same form, the only difference being substituting  $2/(3\sigma ph)$  for  $\gamma$ .

Figs. 5, 6, and 7 show the behavior of the spectral radius of CMFD for various scattering ratios when p=1, p=2, and p=4, respectively, using the  $S_{16}$  Gauss-Legendre quadrature set. Fig. 8 shows the spectral radius of the CMR and the CMFD methods when the scattering ratio is 0.99. The spectral radius of the CMFD method is something like that of the common mesh-centered inconsistent DSA.[13] As the mesh size increases, the spectral radii of the CMFD method also increase similarly as (actually faster than) the CMR method, eventually both becoming unstable (or ineffective). The behavior of coarseness (p) in CMFD is wider in the stable region (lowers the spectral radius below unity) than the fine case (p=1). The coarseness in CMFD also widens the inefficient region as the “spectral wave” moves leftward (Fig. 8). The CMFD method is fast converging as is DSA when the mesh size is small enough, because the spectral radius is less than 0.23.

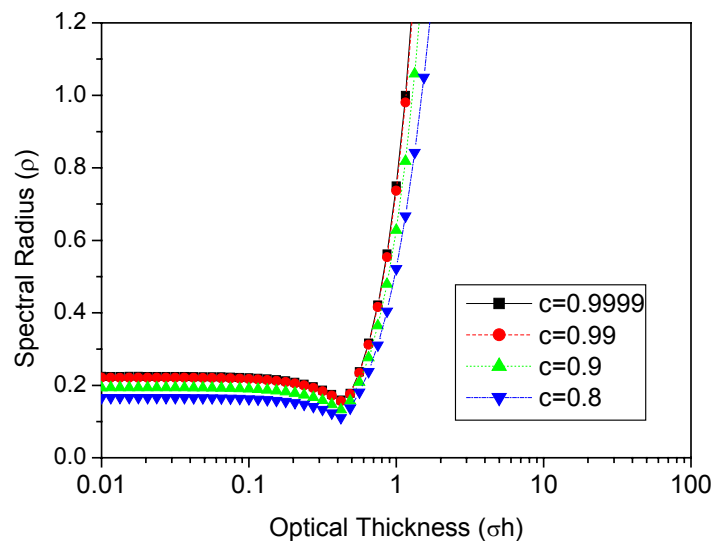


**Fig. 5. Spectral radius of CMFD for various scattering ratios for p=1.**

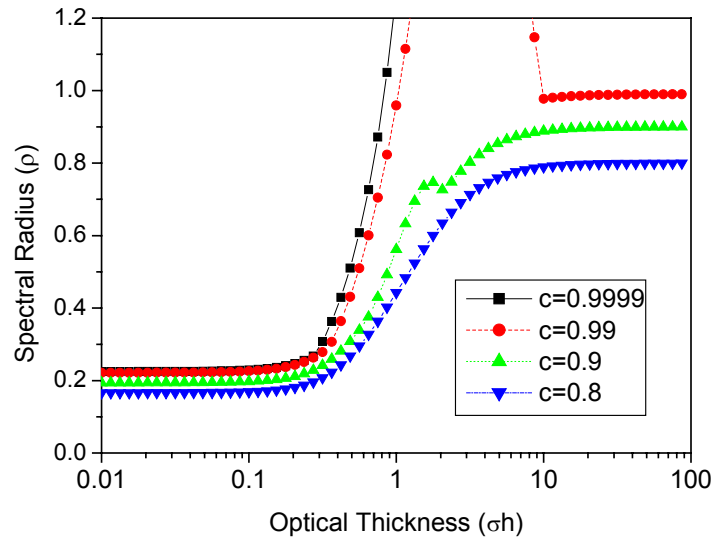


**Fig. 6. Spectral radius of CMFD for various scattering ratios for  $p=2$ .**

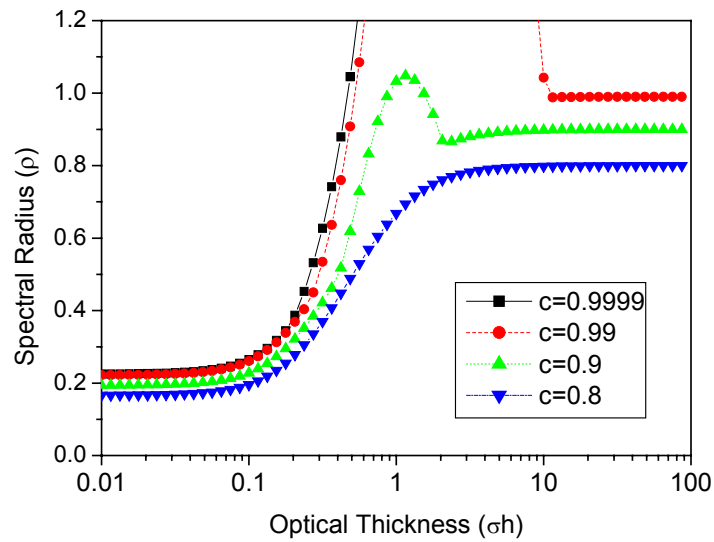


**Fig. 7. Spectral radius of CMFD for various scattering ratios for  $p=4$ .**

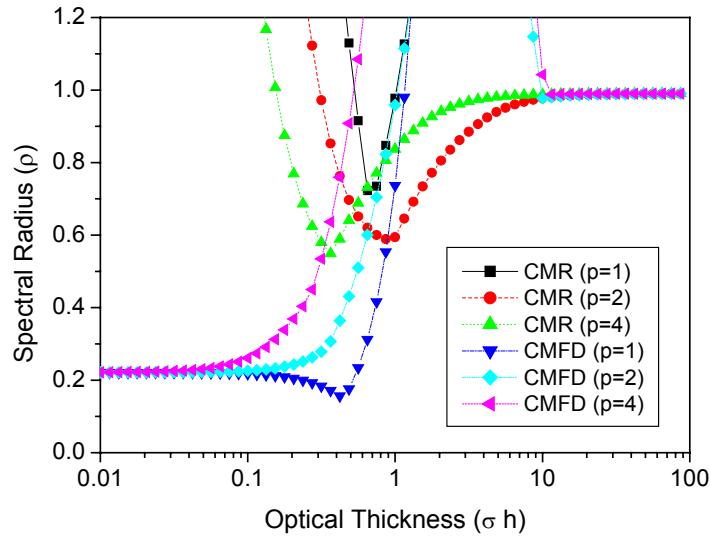


Fig. 8. Spectral radius of CMR and CMFD for various  $p$ 's ( $c=0.99$ ).

#### 4. NUMERICAL COMPARISONS OF CMR AND CMFD

##### 4.1. Consistency of Solutions

When an acceleration method is considered, it is important to check whether the converged solution of the low-order equation (acceleration equation) is the same as that of the high-order equation (transport equation) and identical to the unaccelerated solution. The CMR method clearly has such a consistency of solutions because it uses spatial balance without additional approximation. But the CMFD method uses mesh-average scalar fluxes as unknowns and thus requires careful treatment of the boundary conditions, particularly the vacuum boundary condition; otherwise it may break the consistency. The treatment of Eq. (18) based on the CMR factor concept ensures the consistency. For numerical demonstration, two kinds of tests are performed. The first test is a mono-energy, homogeneous, isotropic, one slab problem which is depicted in Fig. 9.

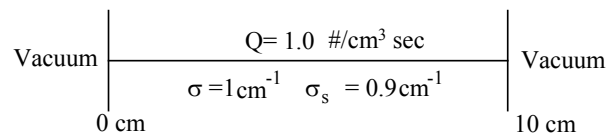


Fig. 9. Configuration of test problem 1.

Vacuum boundary conditions are imposed on both sides and the problem size is 10 cm. The convergence criterion is  $1.0E-9$  for the maximum pointwise scalar flux. Diamond differencing (DD) scheme is considered for spatial discretization and  $S_{16}$  Gauss-Legendre quadrature is used. The mesh size is 1 cm and numbers of coarse meshes are chosen as 5 and 10 and thus the corresponding numbers of fine meshes are 2 and 1, respectively. Table I shows the solutions of source iteration (SI), CMR, and CMFD. Source iteration (SI) uses the solution of the high-order

equation as the next iteration without any low-order equations. Thus the solution of SI means no acceleration. From Table I, we note that there are no differences among SI, CMR, and CMFD solutions even with different coarse meshes.

**Table I. Scalar flux distribution for various methods**

Methods	SI	CMR (high-order)	CMR (low-order)	CMFD (high-order)	CMFD (low-order)
# of iterations	144	(32 <sup>a</sup> , 24 <sup>b</sup> )		(22, 33)	
Mesh 1	4.320019	4.320018	4.320019	4.320018	4.320019
Mesh 2	6.873371	6.873370	6.873370	6.873370	6.873370
Mesh 3	8.054203	8.054202	8.054202	8.054202	8.054202
Mesh 4	8.753147	8.753145	8.753145	8.753145	8.753145
Mesh 5	9.027606	9.027604	9.027604	9.027604	9.027604
Mesh 6	9.027606	9.027604	9.027604	9.027604	9.027604
Mesh 7	8.753147	8.753145	8.753145	8.753145	8.753145
Mesh 8	8.054203	8.054202	8.054202	8.054202	8.054202
Mesh 9	6.873371	6.873370	6.873370	6.873370	6.873370
Mesh 10	4.320019	4.320018	4.320019	4.320018	4.320019

<sup>a</sup>: Number of iterations for 10 coarse meshes,

<sup>b</sup>: Number of iterations for 5 coarse meshes.

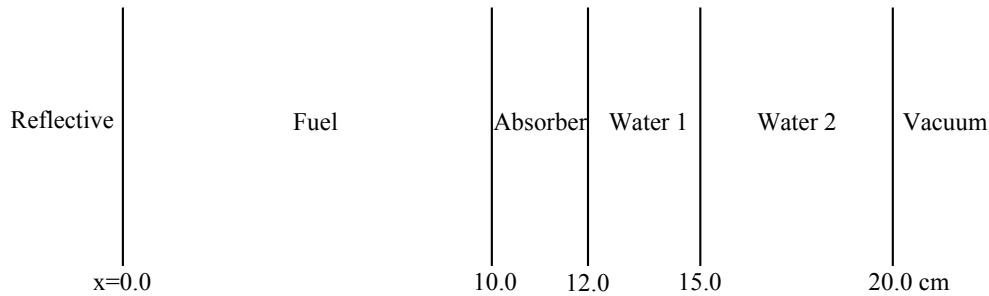


**Fig. 10. Configuration of test problem 2.**

**Table II. Cross sections for materials**

	Group	$\sigma_g$	$\sigma_{0g->1}$	$\sigma_{0g->2}$	$\sigma_{1g->1}$	$\sigma_{1g->2}$	$q_g$
Fuel	1	0.3	0.27	0.01	0.09	0.002	$5\sin(\pi x/10)$
	2	1.0	0.001	0.9	0.0002	0.08	0
Absorber	1	0.2	0.18	0.01	0.08	0.003	0
	2	3.53	0.001	0.53	0.0003	0.06	0
Water 1	1	0.401	0.32	0.08	0.07	0.003	5
	2	1.30	0.002	1.29	0.0004	0.2	5
Water 2	1	0.401	0.32	0.08	0.07	0.003	0
	2	1.30	0.002	1.29	0.0004	0.2	0

The second test is a two-group, heterogeneous, anisotropic, multi-slab problem as shown in Fig. 10. Table II shows the cross sections for each material. Convergence criterion is  $1.0E-6$  and the diamond differencing (DD) scheme is used with  $S_8$  Gauss-Legendre quadrature. Fig. 11 shows the distribution of fast scalar flux and Fig. 12 shows the distribution of thermal scalar flux. For this test problem 2, the analytic solutions (spatial truncation error-free) are provided by IMGF.[14] Table III shows the fast and thermal flux from SI, CMR, and CMFD. We note that both CMR and CMFD have the consistency of solutions.

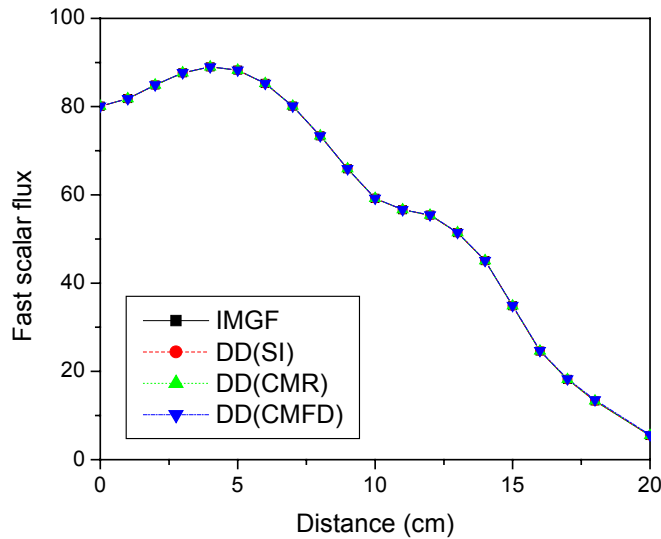


**Fig. 11. Distribution of fast scalar flux for various methods.**

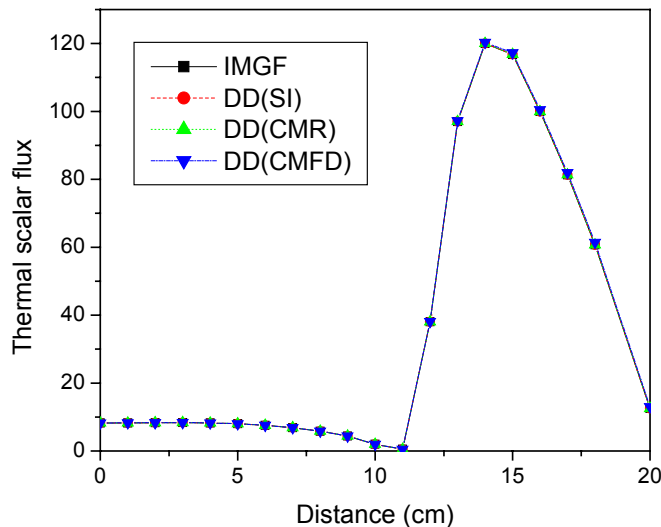


**Fig. 12. Distribution of thermal scalar flux for various methods.**

**Table III. Fast and thermal flux solutions by various methods**

x (cm)	Fast scalar flux				Thermal scalar flux			
	IMGF	DD(SI)	DD(CMR)	DD(CMFD)	IMGF	DD(SI)	DD(CMR)	DD(CMFD)
0	80.0821	80.08967	80.08968	80.08968	8.24275	8.24354	8.24354	8.24354
1	81.7739	81.77441	81.77442	81.77442	8.27467	8.27525	8.27525	8.27525
2	84.8993	84.89926	84.89927	84.89927	8.33493	8.33526	8.33526	8.33526
3	87.6545	87.65400	87.65401	87.65401	8.35586	8.35603	8.35603	8.35603
4	88.9791	88.97816	88.97817	88.97817	8.27073	8.27085	8.27086	8.27086
5	88.2545	88.25319	88.25320	88.25320	8.02301	8.02321	8.02321	8.02321
6	85.2486	85.24730	85.24730	85.24730	7.56696	7.56738	7.56738	7.56738
7	80.1082	80.10713	80.10714	80.10714	6.86103	6.86177	6.86177	6.86177
8	73.3524	73.35152	73.35153	73.35153	5.85031	5.85146	5.85146	5.85146
9	65.8901	65.88962	65.88963	65.88963	4.42285	4.42528	4.42528	4.42528
10	59.1947	59.19892	59.19893	59.19893	1.99504	1.99498	1.99498	1.99498
11	56.6129	56.61649	56.61650	56.61651	0.54028	0.53692	0.53692	0.53692
12	55.4018	55.40516	55.40517	55.40517	38.0336	38.03395	38.03418	38.03418
13	51.4168	51.42089	51.42091	51.42091	97.0065	97.01582	97.01651	97.01649
14	45.0571	45.06128	45.06130	45.06130	119.999	119.9953	119.9963	119.9963
15	34.8274	34.82835	34.82837	34.82836	116.781	116.7853	116.7865	116.7864
16	24.5941	24.59202	24.59203	24.59202	99.9597	99.96303	99.9643	99.9643
17	18.1426	18.14178	18.14180	18.14178	81.3391	81.34252	81.34367	81.34369
18	13.2847	13.28441	13.28442	13.28440	60.7159	60.71869	60.71960	60.71965
20	5.44722	5.44691	5.44691	5.44690	12.5308	12.53137	12.53156	12.53157

**4.2. Convergence of Solutions**

To check the convergence, the numerical spectral radius and the number of iterations are compared for CMR and CMFD methods. The matrix forms of CMR and CMFD are in tri-diagonal form in slab geometry. Therefore, the CMR and CMFD equations are directly solved. Test problem 1 is considered. Fourier analysis is confirmed with various cases of coarseness and various scattering ratios. Tables IV, V, and VI show the numerical spectral radii and the number of iterations for  $p=1$ ,  $p=2$ , and  $p=4$ , respectively. These results indicate the CMFD method has better convergence than the CMR method when the mesh size is small, but for a large mesh size the two methods exhibit similarly divergent behavior. These results are in agreement with the Fourier analysis.

**Table IV. Number of iterations and numerical spectral radius (p=1)**

$\sigma h^a$ ( $I^b$ )	Source Iteration			CMR			CMFD		
	c=0.8 <sup>c</sup>	c=0.9	c=1.0	c=0.8	c=0.9	c=1.0	c=0.8	c=0.9	c=1.0
0.01 (1000)	79 <sup>d</sup> 0.7806 <sup>c</sup>	145 0.8781	684 0.9757	N.C. <sup>f</sup>	N.C.	N.C.	11 0.1526	12 0.1792	13 0.2061
0.02 (500)	79 0.7806	145 0.8781	694 0.9757	N.C.	N.C.	N.C.	11 0.1525	12 0.1791	13 0.2087
0.1 (100)	79 0.7806	145 0.8781	694 0.9757	147 0.9097	N.C.	N.C.	11 0.1494	12 0.1758	13 0.2051
0.2 (50)	79 0.7806	145 0.8781	693 0.9757	32 0.6178	139 0.8947	N.C.	11 0.1402	12 0.1661	13 0.1947
1.0 (10)	78 0.7803	144 0.8779	686 0.9754	24 0.4494	32 0.5551	51 0.6881	18 0.3335	22 0.4041	28 0.4872
2.0 (5)	78 0.7797	143 0.8772	665 0.9746	53 0.6926	199 0.9071	N.C.	N.C.	N.C.	N.C.

<sup>a</sup>: Total cross section ( $\sigma$ ) x Mesh size of fine mesh (h), <sup>b</sup>: Number of coarse meshes,  
<sup>c</sup>: Scattering ratio, <sup>d</sup>: Number of iterations, <sup>e</sup>: Numerical spectral radius, <sup>f</sup>: Not converged.

**Table V. Number of iterations and numerical spectral radius (p=2)**

$\sigma h^a$ ( $I^b$ )	CMR			CMFD		
	c=0.8	c=0.9	c=1.0	c=0.8 <sup>d</sup>	c=0.9	c=1.0
0.01 (500)	N.C. <sup>c</sup>	N.C.	N.C.	11 <sup>e</sup> 0.1526 <sup>f</sup>	12	13
0.02 (250)	N.C.	N.C.	N.C.	11 0.1527	12 0.1793	13 0.2088
0.1 (50)	34 0.6300	163 0.9098	N.C.	11 0.1553	12 0.1828	13 0.2112
0.2 (25)	17 0.3419	31 0.5667	86 0.8066	11 0.1654	12 0.1929	14 0.2241
1.0 (5)	21 0.4171	24 0.4820	31 0.5687	21 0.4723	33 0.5588	28 0.4872
2.5 (2)	36 0.5834	46 0.6563	64 0.7292	36 0.5834	46 0.6563	N.C.

<sup>a</sup>: Total cross section ( $\sigma$ ) x Mesh size of fine mesh (h), <sup>b</sup>: Number of coarse meshes,  
<sup>c</sup>: Not converged, <sup>d</sup>: Scattering ratio, <sup>e</sup>: Number of iterations, <sup>f</sup>: Numerical spectral radius.

**Table VI. Number of iterations and numerical spectral radius (p=4)**

$\sigma h^a$ ( $I^b$ )	CMR			CMFD		
	c=0.8	c=0.9	C=1.0	c=0.8 <sup>d</sup>	c=0.9	c=1.0
0.01 (250)	N.C. <sup>c</sup>	N.C.	N.C.	11 <sup>e</sup> 0.1528 <sup>f</sup>	12 0.1795	13 0.2089
0.02 (125)	N.C.	N.C.	N.C.	11 0.1536	12 0.1804	13 0.2098
0.05 (50)	34 0.6322	169 0.9127	N.C.	11 0.1590	12 0.1869	14 0.2174
0.1 (25)	18 0.3614	32 0.5706	90 0.8136	12 0.1806	13 0.2096	14 0.2426
0.625 (4)	29 0.5467	35 0.6189	46 0.6867	29 0.5414	48 0.6613	N.C.
0.8333 (3)	31 0.5374	40 0.6128	56 0.6994	33 0.5886	166 0.8912	N.C.
1.25 (2)	45 0.6572	62 0.7394	97 0.8216	45 0.6572	62 0.7394	N.C.

<sup>a</sup>: Total cross section ( $\sigma$ ) x Mesh size of fine mesh (h), <sup>b</sup>: Number of coarse meshes,  
<sup>c</sup>: Not converged, <sup>d</sup>: Scattering ratio, <sup>e</sup>: Number of iterations, <sup>f</sup>: Numerical spectral radius.

### 5. CONCLUSIONS

The coarse mesh rebalance (CMR) and coarse mesh finite difference (CMFD) methods are appealing acceleration methods for the neutron transport calculations. This is because it is extremely simple to apply them regardless of the discretization schemes of the transport equation. The coarse mesh can be chosen conveniently as simple in shape and size and overlaid on the fine meshes. The fine meshes inside a coarse mesh can be irregular and unstructured, depending on the solution scheme of the transport sweep.

This paper presented convergence analyses (linearized Fourier analyses) of the two acceleration methods with comparison. As is known in the literature, CMR is conditionally stable in that it is unstable for mesh size too small or too large. As the number of fine meshes in a coarse mesh increases, CMR tends to be stable but becomes inefficient. The results of the study in this paper show for the CMFD method that it is also conditionally stable (in a companion paper[15] in this Proceedings, an unconditionally stable coarse-mesh acceleration method is described). The behavior of coarseness (p) of CMFD is similar to that of CMR. The behavior of the spectral radius of the CMFD method is reminiscent of and similar to that of the inconsistent DSA. The CMFD method is fast converging when the mesh size is small as is DSA, but it becomes divergent or ineffective as the mesh size increases as does CMR. These results of convergence analyses are in agreement with the numerical results of the test problems solved. Similar results are also obtained for eigenvalue problems.

### ACKNOWLEDGMENT

This work was supported in part by the Ministry of Science and Technology of Korea through the National Research Laboratory (NRL) Program.



## REFERENCES

1. N.Z. Cho, G.S. Lee, and C.J. Park, "Fusion of Method of Characteristics and Nodal Method for 3-D Whole-Core Transport Calculation," *Trans. Am. Nucl. Soc.*, **86**, 322 (2002).
2. N.Z. Cho, G.S. Lee, and C.J. Park, "A Fusion Technique of 2-D/1-D Methods for Three-Dimensional Whole-Core Transport Calculations," *Proc. Korean Nuclear Society Spring Meeting*, Kwangju, Korea, May 2002.
3. E.E. Lewis and W.F. Miller, Jr., *Computational Methods of Neutron Transport*, John Wiley & Sons, 1984.
4. G.S. Lee, N.Z. Cho, and S.G. Hong, "Acceleration and Parallelization of the Method of Characteristics for Lattice and Whole-Core Heterogeneous Calculations," *Proc. Int. Mtg. Advances in Reactor Physics and Mathematics and Computations into the New Millennium (PHYSOR 2000)*, Pittsburgh, USA, May 7-11, 2000, p.2301, CD-rom, American Nuclear Society (2000).
5. K.S. Smith, "Nodal Method Storage Reduction by Nonlinear Iteration," *Trans. Am. Nucl. Soc.*, **44**, 265 (1983).
6. P.J. Turinsky, et al., "NESTLE: A Few-Group Neutron Diffusion Equation Solver" EGG-NRE-11406, Electric Power Research Center, North Carolina State University (1994).
7. K.S. Moon, et al., "Acceleration of the Analytic Function Expansion Nodal Method by Two-Factor Two-Node Nonlinear Iteration," *Nucl. Sci. Eng.*, **132**, 194 (1999).
8. K.S. Smith and J.D. Rhodes III, "CASMO Characteristics Method for Two-Dimensional PWR and BWR Core Calculations," *Trans. Am. Nucl. Soc.*, **83**, 294 (2000).
9. K.S. Smith and J.D. Rhodes, III, "Full-Core, 2-D, LWR Core Calculations with CASMO-4E," *Proc. Int. Conf. New Frontiers of Nuclear Technology: Reactor Physics, Safety and High-Performance Computing (PHYSOR 2002)*, Seoul, Korea, October 7-10, 2002, CD-rom, American Nuclear Society (2002).
10. J.Y. Cho, et. al., "Cell Based CMFD Formulation for Acceleration of Whole-Core Method of Characteristics Calculations," *Journal of the Korean Nuclear Society*, **34**, 250 (2002).
11. H.G. Joo, et. al., "Dynamic Implementation of the Equivalence Theory in the Heterogeneous Whole Core Transport Calculation," *Proc. Int. Conf. New Frontiers of Nuclear Technology: Reactor Physics, Safety and High-Performance Computing (PHYSOR 2002)*, Seoul, Korea, October 7-10, 2002, CD-rom, American Nuclear Society (2002).
12. G.R. Cefus and E.W. Larsen, "Stability Analysis of Coarse-Mesh Rebalance," *Nucl. Sci. Eng.*, **105**, 31 (1990).
13. M.L. Adams and E.W. Larsen, "Fast Iterative Methods for Discrete-Ordinates Particle Transport Calculations", *Prog. Nucl. Energy*, **40**, 3 (2002).
14. S.G. Hong and N.Z. Cho, "The Infinite Medium Green's Function Method for Multigroup Discrete Ordinates Transport Problems in Multi-Layered Slab Geometry," *Ann. Nucl. Energy*, **28**, 1101 (2001).
15. Y.R. Park and N.Z. Cho, "Angular Dependent Coarse-Mesh Rebalance Method for Acceleration of the Discrete Ordinates Neutron Transport Calculations," *in this Proceedings*.